
LINC: Decoupling Local Consequence Scoring from Hidden Matching in Constructive Neural Routing

Shaofeng Qin, Li Wang*

Beijing University of Posts and Telecommunications

elaina20041017@gmail.com wang_li@bupt.edu.cn

Abstract

Constructive neural routing solvers usually score the next action by matching a decoder context to candidate embeddings, hiding deterministic one-step consequences such as travel, waiting, slack, and capacity changes. We propose LINC (Local Inference via Normed Comparison), a decoder-side candidate decision architecture that computes these consequences explicitly. LINC uses them according to their decision role: centered relative consequences are compared by a shared linear local scorer, while feasible-set summaries modulate the decoder context. This preserves standard global matching and relieves the hidden state from rediscovering transition arithmetic. The Capacitated Vehicle Routing Problem with Time Windows (CVRPTW) serves as the main constrained-routing stress test; the same interface extends to the Capacitated Vehicle Routing Problem (CVRP) and Traveling Salesman Problem (TSP). In particular, for CVRPTW, LINC reduces PolyNet’s Solomon/Homberger gaps from 13.83%/38.15% to 7.26%/14.71%; for TSP and CVRP, it also improves external-benchmark gaps.

1 Introduction

Constructive neural combinatorial optimization (NCO) has become a standard learning-based paradigm for routing problems: a policy builds a solution one action at a time, and a decoder scores the feasible next nodes conditioned on the partial tour. Starting from pointer-network and attention-model formulations (Vinyals et al., 2015; Bello et al., 2017; Nazari et al., 2018; Kool et al., 2019), later work improved exploration and inference through multi-start rollouts, population policies, and guided search (Kwon et al., 2020; Grinsztajn et al., 2023; Chalumeau et al., 2023; Hottung et al., 2025; Choo et al., 2022). These techniques have made neural constructors competitive on many synthetic TSP and CVRP settings.

The remaining failure mode is most visible when selecting an action sets off a cascade of *state-dependent consequences* that the environment already computes but the network must reconstruct from scratch. In CVRPTW, picking a customer determines arrival time, waiting time, service start, departure, remaining capacity, and the updated time budget constraining all later feasibility checks. None of these are latent: they follow deterministically from the MDP transition. Yet a conventional attention decoder receives none of them directly—it must recover travel cost, timing slack, and capacity pressure through a single hidden context vector, effectively relearning arithmetic the environment already performed. This burden compounds under distribution shift, where the same hidden representation must simultaneously encode global routing strategy and precise local feasibility consequences.

This paper argues that candidate scoring should be treated as a *local comparison problem*. The absolute value of a candidate’s travel time or slack is informative, but the decision often depends on how that value compares with the other feasible candidates at the same step. A set of candidates may

*Corresponding author. Code: <https://github.com/Elaina10172004/LINC>

all be far from the current node, all have late time windows, or all have similarly loose slack. The network should not need to rediscover these common-mode properties through hidden matching—they are already available from the state and transition. For candidate-relative ranking, what matters is often the deviation from the current feasible set: “shorter than the current alternatives”, “tighter than the current alternatives”.

We propose LINC (Local Inference via Normed Comparison), a candidate decision architecture for constructive routing. LINC explicitly computes local consequence features for each feasible candidate, centers the relative features over the feasible customer set, summarizes the step-level candidate set, and combines the result with standard context-key attention. The result is a decoder that still performs global matching through learned embeddings, but no longer asks a single hidden vector to implicitly rediscover elementary transition quantities at every step.

CVRPTW is the primary testbed because it couples geometry, capacity, and temporal feasibility; TSP and CVRP are included to test whether the same interface remains useful when constraints are simpler. The strongest empirical gains occur on CVRPTW: on Solomon and Homberger external benchmarks, LINC reduces the unguided gap from 13.83%/38.15% to 7.26%/14.71% relative to the strongest neural baseline. On random TSP/CVRP, strong baselines are already optimal or nearly optimal, so the residual headroom is small by construction. We therefore evaluate these tasks in two roles: saturated in-distribution checks, where LINC should not damage a near-converged constructive policy, and external/cross-scale checks, where local consequence comparison should reduce the remaining generalization gap. This frames the main contribution as an architecturally decoupled decoder: deterministic local consequences are computed explicitly, with relative consequences compared through a provably invariant linear coordinate, while global state context is routed through learned non-linear modulation—a separation between what can be computed and what must be learned.

Our contributions are:

1. We decouple one-step deterministic transition consequences from latent neural matching: the environment computes exact timing and travel effects, the decoder state and mask handle feasibility and capacity, and the resulting decision signal is factorized into a linear comparison channel and a non-linear modulation path.
2. We formalize the local comparison branch as a canonical consequence comparator: relative consequence tables decompose into candidate-varying contrasts and candidate-common regime statistics; under linearity, permutation equivariance, and the zero-mean softmax gauge, the canonical local scorer takes the centered shared-linear form (Appendix A).
3. We evaluate LINC on CVRPTW, CVRP, and TSP with unguided and SGBS-guided decoding, external benchmarks, and ablations supporting that the decoupled local-consequence interface and step-level summary are central to the gains.

2 Related Work

Constructive neural routing solvers. Pointer Networks introduced sequence-to-sequence construction for combinatorial optimization (Vinyals et al., 2015), followed by reinforcement-learning solvers for TSP and VRP (Bello et al., 2017; Nazari et al., 2018). The Attention Model (AM) (Kool et al., 2019) established the encoder-decoder template that remains the default baseline for routing NCO. POMO (Kwon et al., 2020) exploited multiple equivalent starting solutions to reduce policy-gradient variance and improve inference through multi-start rollouts. LINC is compatible with this constructive setup: it does not change the MDP or add local search operators, but changes the candidate scoring interface used at each autoregressive step.

Diversity, populations, and guided inference. A major line of work improves neural solvers by expanding the set of trajectories considered during training or inference. Population policies and winner-take-all objectives encourage complementary strategies (Grinsztajn et al., 2023; Hottung et al., 2025), while latent-space policy adaptation searches over policy variants at test time (Chalumeau et al., 2023). Guided neural decoding methods such as SGBS, DPDP, MDAM, DACT, and NeuroLKH combine learned signals with beam search, dynamic programming, improvement, or LKH-style inference (Choo et al., 2022; Kool et al., 2022; Xin et al., 2021a; Ma et al., 2021; Xin et al., 2021b).

These methods answer “which trajectories should be explored?” LINC addresses a different question: given a particular partial solution and feasible set, what information should the decoder compare before assigning logits?

Generalization and decoder bottlenecks. Several recent papers argue that constructive NCO fails out of distribution because the model retains decision-irrelevant information or places too much burden on static embeddings. BQ-NCO formalizes a bisimulation quotient for constructive MDPs, showing how removing irrelevant state distinctions can improve generalization (Drakulic et al., 2023). LEHD shifts capacity from a light encoder to a heavier decoder for large-scale generalization (Luo et al., 2023), and ReLD re-examines light-decoder solvers, arguing that static embeddings become too dense as VRP complexity increases (Huang et al., 2025). LINC is closest in motivation to this decoder-bottleneck view, but its mechanism is different: rather than only increasing decoder capacity, it externalizes transition-coupled candidate consequences and routes them through a decoupled comparison-and-modulation interface. Centering provides the invariant coordinate for the local comparison subproblem, formalized in Appendix A through a common-mode decomposition and a canonical equivariant linear scorer; unlike BQ-NCO’s full MDP quotienting, this is intentionally local to single-step ranking.

Algorithmic alignment and architectural decoupling. The concept of *algorithmic alignment* (Xu et al., 2020) argues that networks whose computational graph mirrors the target algorithm’s structure generalize better. This principle has been explored through relational graph networks (Battaglia et al., 2018) and symmetry-aware architectures (Bronstein et al., 2021). LINC applies the same philosophy to a local bottleneck: instead of letting a decoder rediscover arrival times, capacity feasibility, and timing slack through hidden vectors—elementary arithmetic the MDP transition already defines—LINC computes these quantities explicitly and separates them into an invariant candidate-comparison coordinate and a state-level context signal.

VRP variants and constraint handling. Another line focuses on broader VRP coverage, robustness, and complex constraints, including omni-generalizable VRP solvers, robust routing policies, complex-constraint handling, decomposed constraint retrieval, and multi-task mixture-of-experts formulations (Zhou et al., 2023, 2024a; Bi et al., 2024; Jiang et al., 2025; Zhou et al., 2024b; Berto et al., 2025). These works seek variant-level generality or robustness across problem families. LINC makes a more modest and explicit design choice: for each routing variant, we expose the local consequences that are physically meaningful for that variant. This improves interpretability and constrained-decision quality, but it is not a task-agnostic universal solver. Relative to this literature, LINC changes the one-step scoring interface rather than the search procedure.

3 Problem Setup and Framework

3.1 Background

We follow the standard constructive NCO formulation: a solution is built sequentially as $\xi_{\leq t} = (a_1, \dots, a_t)$, with the policy factorizing as $\pi_\theta(\xi | l) = \prod_t \pi_\theta(a_t | s_t, l)$. TSP, CVRP, and CVRPTW share this autoregressive paradigm but differ in state variables—TSP tracks visited nodes; CVRP adds remaining capacity and depot resets; CVRPTW further adds current time, service times, and customer time windows. We do not alter the MDP definitions or transitions; LINC only changes the decoder-side scoring interface used to assign logits to feasible actions in \mathcal{A}_t .

3.2 LINC Overview

At a high level, LINC augments the base decoder logit $b_{t,j}$ with a state-conditioned local consequence comparator:

$$u_{t,j} = \alpha_t b_{t,j} + v_t^\top \phi_t(j), \tag{1}$$

where $\phi_t(j)$ is the explicit local consequence representation, v_t is a candidate-shared linear comparator, and α_t gates the base matching path. The following sections define $\phi_t(j)$, the feasible-set summary used to condition v_t and α_t , and the implementation parameterization that realizes this interface.

LINC separates two parts of the current-step decision: the learned global matching captured by attention, and the deterministic local consequences of choosing candidate j in state s_t —travel increment, waiting, slack, arrival/departure timing, and task-specific cues. Some of these features are most informative as absolute quantities, while others matter through their deviation from the current feasible set.

The resulting interface has three components, but its novelty lies not in what features are provided but in *how* they are used. LINC factorizes exact local consequence quantities into two distinct roles: candidate-level deviations are scored through a shared linear comparator for relative ranking, while feasible-set aggregates modulate the decoder context to reflect global urgency. Table 2 summarizes this decoupling: the two channels converge into a single final score, but their computational responsibilities are separated—what the environment already defines is computed, not rediscovered through hidden matching.

Unlike merely adding static feature augmentation (e.g., KNN distances), LINC’s local-consequence features are action-effect quantities induced by the known transition: “if candidate j is selected now, how will the routing state change?” This follows the principle of *algorithmic alignment* by explicitly computing deterministic consequences of state transitions rather than learning them, preserving network capacity for high-level routing strategy. LINC thus interfaces with the known MDP transition as an external consequence computer, rather than training a network to approximate that computation.

3.3 Candidate-Level Comparison Channel

Let \mathcal{A}_t be the full feasible action set (including the depot when allowed), and $F_t \subseteq \mathcal{A}_t$ the feasible customer subset used for centering. The policy is defined over \mathcal{A}_t , while the equivariant formalization applies to the exchangeable customer rows in F_t . The depot is a distinguished return action: its raw relative vector is zero before centering, so its centered coordinate is measured against the customer mean; depot feasibility and route-reset semantics remain handled by the decoder state and mask. For each $j \in F_t$, we partition the explicit candidate features into an absolute subset $x_{\text{abs},t}(j)$ and a relative subset $x_{\text{rel},t}(j)$. For CVRPTW, the relative subset includes normalized travel time, waiting time, time-window slack ratio, arrival time, and departure time; the absolute subset retains non-centered geometric cues such as angular direction. Capacity and feasibility are handled by the decoder state and mask, with task-specific regime quantities routed through the summary when applicable. Feature definitions for each task are given in Table 1.

If $F_t = \emptyset$, set $\mu_t = 0$ and use a zero summary. Otherwise,

$$\mu_t = \frac{1}{|F_t|} \sum_{u \in F_t} x_{\text{rel},t}(u). \quad (2)$$

For $j \in F_t$, set $\bar{x}_{\text{rel},t}(j) = x_{\text{rel},t}(j) - \mu_t$, and for the depot, when available, $\bar{x}_{\text{rel},t}(\text{depot}) = -\mu_t$. Thus, customer-common offsets are removed from customer-to-customer ranking but can still inform the special depot-vs-customer decision. The final candidate representation used for dynamic scoring is

$$\phi_t(j) = [x_{\text{abs},t}(j); \bar{x}_{\text{rel},t}(j)], \quad (3)$$

where for the depot the absolute block is zero by convention; the formal results below concern only the customer rows.

Let $X_t \in \mathbb{R}^{|F_t| \times p}$ stack the relative features of the feasible customers and let $C_t(X_t) = X_t - \mathbf{1}\mu_t^\top$. Set-relative centering removes common feasible-set translations: $C_t(X_t + \mathbf{1}\delta^\top) = C_t(X_t)$. Appendix A formalizes two consequences of this decomposition: C_t is the canonical representative after removing common translations (A.1), and the centered shared-linear scorer is the canonical linear permutation-equivariant scorer in the zero-mean softmax gauge (A.2).

This result directly shapes the relative comparison branch. Since the affine local-advantage interpretation requires a candidate-shared linear weight, LINC scores the explicit candidate representation through a shared linear projection W_ϕ : relative coordinates are centered before scoring, while absolute cues enter the same candidate-shared comparator. A nonlinear candidate-wise MLP preserves translation invariance on centered relative inputs but not the shared comparator structure (validated in Section 4.4).

Conversely, complementary candidate-common information—feasible-set means, minimum slack, feasible-customer ratio—carries global state urgency and is preserved through the step-level summary

Table 1: Task-specific inputs used by LINC.

Task	Relative features	Absolute features	Notes
CVRPTW	travel, wait, slack, arrival, departure	angle; capacity/feasibility via decoder state & mask	Temporal consequences and constraint tightness.
CVRP	travel, demand ratio, dist. to depot	depot angle; capacity/feasibility via decoder state & mask	Load-after ratio in summary; KNN distance as static feature.
TSP	travel	centroid angle; visit mask via decoder state	KNN distance as static feature; no load/time transitions.

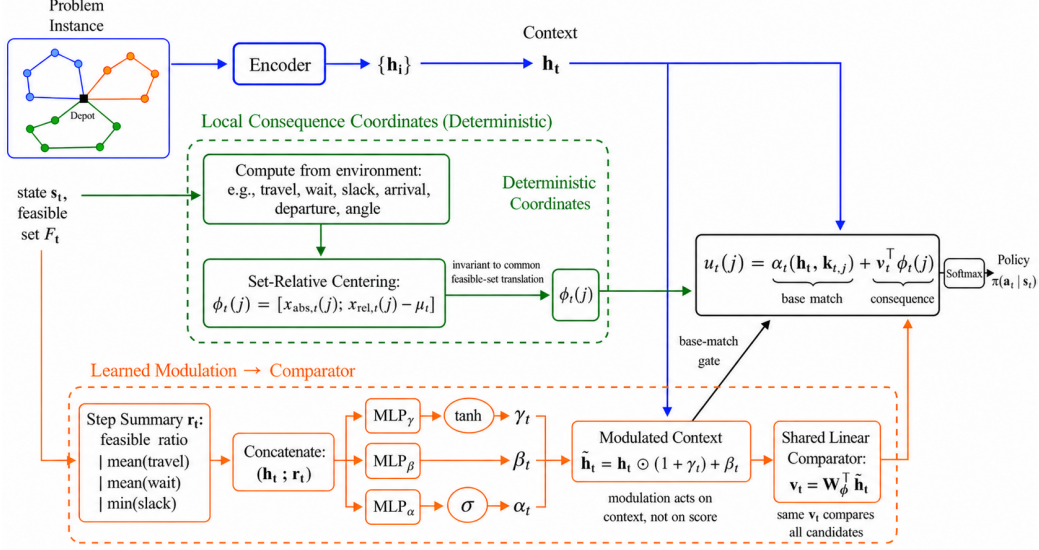


Figure 1: LINC decoder architecture: deterministic local consequence coordinates and a state-conditioned linear comparator are decoupled, with the final score separating computed quantities from learned hidden matching.

r_t , feeding the decoder via learned modulation $\gamma_t, \beta_t, \alpha_t$. This implements a clean decoupling: local comparison on invariant linear coordinates, global context through learned non-linear modulation.

3.4 Network Architecture

Figure 1 illustrates the LINC decoder. Instead of compressing all candidate judgments into standard context–key matching, it explicitly introduces a local consequence branch and a feasible-set summary branch before candidate scoring.

Concretely (using CVRPTW as the running example), the decoder first produces context h_t and candidate keys $k_{t,j}$. In parallel, the local consequence branch constructs an explicit candidate feature vector from state s_t and candidate customer j :

$$x_t(j) = [\hat{c}_t(j), \hat{w}_t(j), \hat{\sigma}_t(j), \widehat{\text{arr}}_t(j), \widehat{\text{dep}}_t(j), \hat{\theta}_t(j)], \quad (4)$$

where $\hat{c}_t(j)$ is normalized travel time, $\hat{w}_t(j)$ is normalized waiting time, $\hat{\sigma}_t(j)$ is normalized time-window slack, $\widehat{\text{arr}}_t(j)$ and $\widehat{\text{dep}}_t(j)$ are normalized arrival and departure times, and $\hat{\theta}_t(j)$ is the angular difference relative to the depot or current heading. Together they capture “what happens immediately if this candidate is chosen”; feasibility and capacity are handled by the decoder state and mask.

All local consequence features are normalized by task-appropriate instance-level scales before scoring; the exact choices follow the released checkpoint protocols and are specified in the reproduction code. These quantities come from deterministic transition equations, not solver labels.

The decoder selects a feature subset, applies the centering of Section 3.3 to the relative features to obtain $\phi_t(j)$, then projects via a linear map W_ϕ to the same dimension as the decoder context. Beyond candidate-level representations, we construct a step-level summary from the current feasible

Table 2: Functional decoupling of computational responsibilities in LINC.

Responsibility	Realized by
Global policy matching	$b_{t,j}$, the standard context–key matching logit
Exact local consequence computation	Environment / deterministic transition equations
Candidate-level consequence comparison	$[x_{\text{abs},t}(j); x_{\text{rel},t}(j)]$ scored by shared linear weight v_t
Feasible-set urgency	Summary r_t
State-conditioned modulation	$\gamma_t, \beta_t, \alpha_t$ from $[h_t; r_t]$; $v_t = W_\phi^\top \tilde{h}_t$

set:

$$r_t = \left[\rho_t, \text{mean}_{j \in F_t}(\hat{c}_t(j)), \text{mean}_{j \in F_t}(\hat{w}_t(j)), \min_{j \in F_t}(\hat{\sigma}_t(j)) \right], \quad (5)$$

where $\rho_t = |F_t| / \max(n, 1)$ is the feasible-customer ratio (excluding the depot). Across tasks, r_t follows the same pattern: feasible-customer ratio, several feature means, and the minimum of a key constraint quantity (load-after ratio for CVRP, slack for CVRPTW).

The context and summary are concatenated and fed through three small MLPs with appropriate activations to produce modulation quantities:

$$\gamma_t = \tanh(\text{MLP}_\gamma([h_t; r_t])), \quad \beta_t = \text{MLP}_\beta([h_t; r_t]), \quad \alpha_t = \sigma(\text{MLP}_\alpha([h_t; r_t])), \quad (6)$$

where $\gamma_t, \beta_t \in \mathbb{R}^d$, $\alpha_t \in (0, 1)$. The \tanh nonlinearity constrains $\gamma_t \in (-1, 1)$ to prevent over-scaling the context, and σ denotes a sigmoid. The modulated context is defined as

$$\tilde{h}_t = h_t \odot (1 + \gamma_t) + \beta_t. \quad (7)$$

The final unnormalized score for candidate j is

$$u_{t,j} = \alpha_t \langle h_t, k_{t,j} \rangle + \langle \tilde{h}_t, W_\phi \phi_t(j) \rangle. \quad (8)$$

The policy is

$$\pi_\theta(a_t = j \mid s_t) = \text{softmax}_{j \in \mathcal{A}_t}(u_{t,j}). \quad (9)$$

The local-comparator term can be written as $\langle \tilde{h}_t, W_\phi \phi_t(j) \rangle = v_t^\top \phi_t(j)$ with $v_t = W_\phi^\top \tilde{h}_t$, so all candidates share the same state-conditioned linear weight. Writing $v_{\text{rel},t}$ for the block of v_t that multiplies the relative coordinates, for customer rows $v_{\text{rel},t}^\top x_{\text{rel},t}(j) = v_{\text{rel},t}^\top (x_{\text{rel},t}(j) - \mu_t) + v_{\text{rel},t}^\top \mu_t$: the second term is constant within F_t and lies in the softmax-gauge direction for customer-to-customer ranking. LINC therefore routes deviations to the shared comparator, regime aggregates to summary modulation, and the depot’s $-\mu_t$ coordinate to the return-vs-customer decision. This consequence-routing decomposition separates LINC from generic feature injection.

When training with a reference policy initialization, we additionally apply score morphing:

$$u_{t,j}^{\text{final}} = u_{t,j}^{\text{ref}} + \lambda_{\text{morph}} (u_{t,j} - u_{t,j}^{\text{ref}}), \quad (10)$$

where $u_{t,j}^{\text{ref}}$ is the reference policy’s score at the same step. λ_{morph} anneals from 0 to 1. TSP and CVRP experiments complete this annealing within the first 100 epochs. For models trained from scratch, $\lambda_{\text{morph}} = 1$ and no reference score mixing is used.

Complexity-wise, let $|\mathcal{A}_t|$ be the feasible action count, d the hidden dimension, p_ϕ the explicit feature dimension. The original context–key matching is $O(|\mathcal{A}_t|d)$; LINC adds $O(|\mathcal{A}_t|p_\phi)$ for feature computation and centering, plus $O(|\mathcal{A}_t|d)$ for feature projection and dynamic scoring. Since $p_\phi \ll d$, per-step candidate scoring remains $O(|\mathcal{A}_t|d)$, and the full construction does not change the dominant order in problem size n .

3.5 Training Strategy and Credit Assignment

LINC is trained using REINFORCE with sampled z -vector rollouts, following the same diversity mechanism as PolyNet (Hottung et al., 2025). For CVRPTW scratch training, we use a matched soft top-1 advantage that anneals from a group-mean baseline to hard top-1; the derivation is in Appendix H. TSP and CVRP are initialized from converged PolyNet weights and use hard top-1, with training focused on adapting the LINC scoring interface through slow-start and score morphing. All neural methods that we retrain (POMO, PolyNet, LINC) use identical data generators and test sets within each task.

¹The scoring equation omits implementation-level projection biases; in the unclipped affine scorer these contribute candidate-independent offsets at a fixed step and are not part of the formal results in Appendix A. The no-bias ablation (+0.07%) confirms they do not drive the reported gains.

4 Experiments

4.1 Problem Definitions and Experimental Setup

We evaluate three Euclidean routing problems: TSP minimizes closed-tour length; CVRP adds depot returns and vehicle capacity; CVRPTW further adds service times and customer time windows. Following PolyNet (Hottung et al., 2025) and standard NCO practice, we optimize total travel distance for CVRPTW.

Random test sets follow the Euclidean setup of (Kool et al., 2019): node coordinates are drawn in the unit square, with training size $n = 100$ for TSP and CVRP, and evaluation at $n = 100$ in-distribution and $n = 150$ cross-scale. External generalization includes TSPLIB50–200, CVRPXML100, and CVRPTW Solomon-100/Homberger-200 (Solomon, 1987). Unless noted, “Obj.” denotes average total distance, and gaps are computed relative to optima, best-known solutions, or the solver reference reported in the table.

We use batch size 128 and rollout width $K = 128$ (full hyperparameters in Appendix E). Appendix G describes minor encoder auxiliary components (GateAttn and Depth Mixer), ablated separately and not part of the proposed scoring interface. For TSP and CVRP, LINC continues training from converged PolyNet weights (initialized from POMO and verified as converged). For CVRPTW, POMO and PolyNet are re-trained from scratch on our programmatic generator (Appendix F) using published recipes, ensuring identical data conditions. Training used a single NVIDIA RTX 5090 32GB GPU; inference timings were measured on a single NVIDIA A100 40GB GPU. Feasibility is enforced at each step by masking infeasible actions; post-hoc verification confirms zero constraint violations in all evaluation runs. Appendix D reports three-seed paired bootstrap checks for small-margin comparisons.

We partition methods into unguided neural constructors (POMO, Poppy, PolyNet, LINC) and guided/search-enhanced methods (SGBS, DPDP, MDAM, DACT, BQ-NCO). For CVRPTW, we use PyVRP (Wouda et al., 2024) as the solver reference under the distance-only objective (following PolyNet-style NCO evaluation); for TSP and CVRP, Concorde/LKH3 and HGS/LKH3 serve as traditional solver references (Applegate et al., 2006; Helsgaun, 2017; Vidal, 2022). Following standard practice (Kwon et al., 2020; Hottung et al., 2025; Chalumeau et al., 2023), we report wall-clock inference time alongside objective gaps.

4.2 CVRPTW Results

CVRPTW simultaneously couples geometry, capacity, and temporal feasibility, making it the most thorough testbed for explicit local consequence modeling. Table 3 reports the benchmark results.

Table 3: Search performance results for CVRPTW benchmarks.

Type	Method	Synthetic-100 10K instances			Solomon-100 56 instances			Homberger-200 60 instances		
		Obj.	Gap	Time	Obj.	Gap	Time	Obj.	Gap	Time
Solver	PyVRP	1857.063	–	14h	973.2	–	28m	2687.7	–	1h
Unguided	POMO (greedy)	2325.943	25.25%	12s	1235.250	26.92%	0.9s	4235.323	57.58%	1s
	POMO (sampling)	2259.117	21.65%	40s	1197.800	23.07%	1s	4063.189	51.18%	3s
	PolyNet	2016.511	8.59%	6m	1107.833	13.83%	3s	3712.766	38.15%	8s
	LINC	1920.443	3.41%	12m	1043.898	7.26%	6s	3083.002	14.71%	15s
Guided	POMO SGBS	1999.730	7.68%	9m	1087.689	11.76%	11s	3482.300	29.57%	1m
	PolyNet SGBS	1970.843	6.13%	9m	1063.502	9.27%	11s	3290.331	22.42%	1m
	LINC SGBS	1897.500	2.18%	16m	1023.829	5.20%	24s	2897.835	7.82%	1m

Figure 2 shows LINC reaching PolyNet’s final performance with substantially fewer training instances. Gains hold across all three benchmark families in both unguided and SGBS-guided decoding. All neural baselines use the same training generator; Solomon and Homberger are external transfer tests. The largest gains appear on Homberger-200, where accumulated timing and capacity consequences are hardest to recover from hidden matching alone.

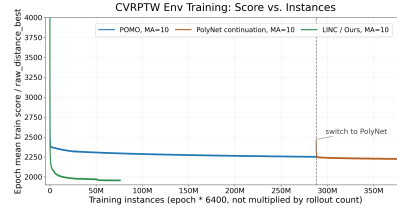


Figure 2: Training curves on the CVRPTW environment dataset.

4.3 TSP and CVRP

We extend LINC to TSP and CVRP to verify generalization under simpler constraint combinations. Both models are initialized from PolyNet n100 weights. For TSP, where there are no load or time-window transitions, LINC reduces to a lightweight geometry-conditioned comparator; the strongest form of deterministic consequence decoupling appears in CVRPTW and CVRP, where actions change capacity or temporal state. For CVRP, LINC uses demand-ratio comparator cues and load-after summary cues to sense capacity exhaustion risk.

Table 4: Search performance results for TSP (top) and CVRP (bottom).

Type	Method	Test			Generalization			External benchmark		
		$n_{tr} = n_{eval} = 100$			$n_{tr} = 100, n_{eval} = 150$			TSPLIB50–200 / CVRPXML100		
		Obj.	Gap	Time	Obj.	Gap	Time	Obj.	Gap	Time
<i>TSP</i>										
Solver	Concorde	7.765	–	82m	9.346	–	17m	30478.9	–	–
	LKH3	7.765	0.000%	8h	9.346	0.000%	99m	30478.9	0.000%	–
Unguided	POMO (greedy)	7.788	0.296%	9s	9.437	0.972%	2s	31650.1	3.84%	15s
	POMO (sampling)	7.775	0.129%	38s	9.393	0.500%	11s	31194.6	2.35%	14s
	Poppy	7.766	0.015%	4m	9.362	0.171%	1m	–	–	–
	PolyNet	7.765	0.000%	4m	9.352	0.064%	1m	31474.2	3.27%	17s
	LINC	7.765	0.000%	8m	9.352	0.061%	2m	31096.3	2.03%	17s
Guided	DPDP	7.765	0.004%	2h	9.434	0.942%	44m	–	–	–
	MDAM	7.781	0.208%	4h	9.403	0.610%	1h	–	–	–
	BQ-NCO	7.766	0.010%	25m	9.351	0.057%	7m	30984.6	1.66%	21s
	POMO SGBS	7.769	0.058%	9m	9.367	0.225%	8m	30748.7	0.89%	2m
	PolyNet SGBS	7.765	0.000%	9m	9.348	0.025%	2m	30909.6	1.41%	2m
	LINC SGBS	7.765	0.000%	12m	9.348	0.021%	3m	30657.3	0.59%	3m
<i>CVRP</i>										
Solver	HGS	15.563	–	54h	19.055	–	9h	16976.434	0.003%	7d
	LKH3	15.646	0.53%	6d	19.222	0.88%	20h	17057.239	0.479%	7d
Unguided	POMO (greedy)	15.969	2.61%	11s	20.054	5.24%	3s	18419.3	8.50%	10s
	POMO (sampling)	15.754	1.23%	47s	19.685	3.31%	14s	17889.4	5.38%	53s
	Poppy	15.685	0.78%	5m	19.578	2.74%	1m	–	–	–
	PolyNet	15.640	0.50%	5m	19.507	2.37%	2m	17632.2	3.87%	7m
	LINC	15.638	0.48%	9m	19.468	2.17%	3m	17518.8	3.20%	14m
Guided	DACT	15.747	1.18%	22h	19.594	2.83%	16h	–	–	–
	DPDP	15.627	0.41%	23h	19.312	1.35%	5h	–	–	–
	MDAM	15.885	2.07%	5h	19.686	3.31%	1h	–	–	–
	BQ-NCO	15.806	1.56%	26m	19.399	1.81%	7m	17947.9	5.73%	26m
	POMO SGBS	15.659	0.62%	10m	19.426	1.95%	4m	17511.0	3.15%	17m
	PolyNet SGBS	15.617	0.35%	12m	19.358	1.59%	3m	17402.5	2.51%	15m
LINC SGBS	15.615	0.33%	18m	19.333	1.46%	5m	17327.5	2.07%	21m	

Random TSP100/CVRP100 are saturated checks where PolyNet already reaches near-zero gaps, so little residual headroom remains. LINC preserves this near-optimal behavior while consistently reducing residual gaps on external benchmarks: on TSPLIB from 3.27% to 2.03% (unguided PolyNet) and 1.41% to 0.59% (PolyNet SGBS); on CVRPXML100 from 3.87% to 3.20% and 2.51% to 2.07%. Appendix D reports paired bootstrap intervals for small-margin TSP/CVRP comparisons and a reduced-budget check ($z = 400$) showing that reduced-budget LINC retains the main external/CVRPTW advantage over full-budget PolyNet.

4.4 Ablation

To analyze the sources of LINC’s gains, we conduct ablations on a simplified CVRPTW dataset. All variants use identical training and validation sets and the same training budget.

The ablations show that the gains do not come from raw feature injection alone. Removing the local consequence interface (2.26%) or replacing it with a naive 2-layer MLP (134→64→1, GELU; 2.31%) costs nearly the same, confirming that what matters is structured routing of consequences by decision role. Removing the step summary (3.15%) is the second-largest penalty, confirming that candidate-common regime information is not disposable.

Raw linear scoring (593.66, +0.25%) stays close to Full LINC because softmax in an affine scorer already cancels candidate-independent shifts on in-distribution data, but explicit centering makes the gauge provable rather than implicit—a structural guarantee that helps prevent common-mode offsets from being absorbed during training and resurfacing as scoring drift under distribution shift. Centered MLP scoring (608.98, +2.83%) retains translation invariance of the centered input, yet degrades substantially because the nonlinear MLP abandons the shared linear comparator structure formalized in Appendix A. This pattern matches the decision-role decoupling view: naive MLP injection re-entangles contrast and regime information, removing the summary discards the candidate-common regime, and centered MLP keeps the coordinate but loses the shared linear comparison geometry. Table 8 reports the full ablation, where GateAttn is neutral and Depth Mixer is smaller than the core local-interface, comparator, and summary removals; pairwise curves are in Appendix C.

4.5 Limitations

LINC inherits the autoregressive POMO/PolyNet-style construction paradigm: it builds from a single partial route prefix, so the decoder cannot fully coordinate multiple routes in parallel and can suffer from early commitment or route imbalance. It also requires meaningful consequence features per variant and is not a task-agnostic universal solver. Appendix A formalizes only a single-step comparator, not full-MDP bisimulation or global optimality. Addressing these limitations likely requires richer vehicle-assignment, multi-depot, or search-augmented construction mechanisms.

5 Conclusion

We presented LINC, a decoder that separates what the routing transition already computes from what the neural policy must learn: candidate-specific contrasts are scored on centered shared-linear coordinates, while global state context flows through nonlinear modulation. Gains are largest when local consequences are central to feasibility (CVRPTW); on saturated random TSP/CVRP, LINC preserves near-optimality and improves residual gaps under external shift. Future work can expose cheap short-horizon consequence summaries through the same decision-role interface, moving from one-step comparison toward predictive local comparison without forcing lookahead arithmetic back into the latent matcher. More broadly, these results support an action-effect decoupling principle in constructive neural decision models: quantities already defined by a known transition, simulator, or constraint process should be computed explicitly and routed according to their decision role, rather than rediscovered through latent matching.

Improved neural constructors for time-windowed logistics may reduce travel distance, fuel use, and operating costs in deployment; risks remain those of standard optimization systems, including dependence on objective design, data quality, and operational constraints.

References

Applegate, D. L., Bixby, R. E., Chvátal, V., and Cook, W. J. *The Traveling Salesman Problem: A Computational Study*. Princeton University Press, 2006.

Variant	Obj.	Rel. gap
Baseline	631.65	6.66%
Full LINC	592.21	0.00%
w/o local consequence interface	605.60	2.26%
Naive MLP injection	605.89	2.31%
Raw linear scoring	593.66	0.25%
Centered MLP scoring	608.98	2.83%
w/o step summary	610.85	3.15%
group_mean	626.37	5.77%

Table 5: Ablation on simplified CVRPTW. Rel. gap is relative to Full LINC.

- Battaglia, P. W., Hamrick, J. B., Bapst, V., Sanchez-Gonzalez, A., Zambaldi, V., Malinowski, M., Tacchetti, A., Raposo, D., Santoro, A., Faulkner, R., et al. Relational inductive biases, deep learning, and graph networks. *arXiv preprint arXiv:1806.01261*, 2018.
- Bello, I., Pham, H., Le, Q. V., Norouzi, M., and Bengio, S. Neural Combinatorial Optimization with Reinforcement Learning. *ICLR*, 2017.
- Berto, F. et al. RL4CO: an Extensive Reinforcement Learning for Combinatorial Optimization Benchmark. *KDD*, 2025.
- Bi, J., Ma, Y., Zhou, J., Song, W., Cao, Z., Wu, Y., and Zhang, J. Learning to Handle Complex Constraints for Vehicle Routing Problems. *NeurIPS*, 2024.
- Bronstein, M. M., Bruna, J., Cohen, T., and Veličković, P. Geometric Deep Learning: Grids, Groups, Graphs, Geodesics, and Gauges. *arXiv preprint arXiv:2104.13478*, 2021.
- Chalumeau, F., Surana, S., Bonnet, C., Grinsztajn, N., Pretorius, A., Laterre, A., and Barrett, T. Combinatorial Optimization with Policy Adaptation using Latent Space Search. *NeurIPS*, 2023.
- Choo, J., Kwon, Y.-D., Kim, J., Jae, J., Hottung, A., Tierney, K., and Gwon, Y. Simulation-guided Beam Search for Neural Combinatorial Optimization. *NeurIPS*, 2022.
- Drakulic, D., Michel, S., Mai, F., Sors, A., and Andreoli, J.-M. BQ-NCO: Bisimulation Quotienting for Efficient Neural Combinatorial Optimization. *NeurIPS*, 2023.
- Grinsztajn, N., Furelos-Blanco, D., Surana, S., Bonnet, C., and Barrett, T. Winner Takes It All: Training Performant RL Populations for Combinatorial Optimization. *NeurIPS*, 2023.
- Helsgaun, K. An Extension of the Lin-Kernighan-Helsgaun TSP Solver for Constrained Traveling Salesman and Vehicle Routing Problems. Technical Report, Roskilde University, 2017.
- Hottung, A., Mahajan, M., and Tierney, K. PolyNet: Learning Diverse Solution Strategies for Neural Combinatorial Optimization. *ICLR*, 2025.
- Huang, Z., Zhou, J., Cao, Z., and Xu, Y. Rethinking Light Decoder-based Solvers for Vehicle Routing Problems. *ICLR*, 2025.
- Jiang, X., Wu, Y., Zhang, C., and Zhang, Y. DRoC: Elevating Large Language Models for Complex Vehicle Routing via Decomposed Retrieval of Constraints. *ICLR*, 2025.
- Kool, W., van Hoof, H., and Welling, M. Attention, Learn to Solve Routing Problems! *ICLR*, 2019.
- Kool, W., van Hoof, H., Gromicho, J., and Welling, M. Deep Policy Dynamic Programming for Vehicle Routing Problems. *CPAIOR*, 2022.
- Kwon, Y.-D., Choo, J., Kim, B., Yoon, I., Gwon, Y., and Min, S. POMO: Policy Optimization with Multiple Optima for Reinforcement Learning. *NeurIPS*, 2020.
- Luo, F., Lin, X., Liu, F., Zhang, Q., and Wang, Z. Neural Combinatorial Optimization with Heavy Decoder: Toward Large Scale Generalization. *NeurIPS*, 2023.
- Ma, Y., Li, J., Cao, Z., Song, W., Zhang, L., Chen, Z., and Tang, J. Learning to Iteratively Solve Routing Problems with Dual-Aspect Collaborative Transformer. *NeurIPS*, 2021.
- Nazari, M., Oroojlooy, A., Snyder, L. V., and Takáč, M. Reinforcement Learning for Solving the Vehicle Routing Problem. *NeurIPS*, 2018.
- Solomon, M. Algorithms for the Vehicle Routing and Scheduling Problems with Time Window Constraints. *Operations Research*, 35(2):254–265, 1987.
- Vidal, T. Hybrid Genetic Search for the CVRP: Open-Source Implementation and SWAP* Neighborhood. *Computers & Operations Research*, 140:105643, 2022.
- Vinyals, O., Fortunato, M., and Jaitly, N. Pointer Networks. *NeurIPS*, 2015.

- Wouda, N. A., Lan, L., and Kool, W. PyVRP: a high-performance VRP solver package. *INFORMS Journal on Computing*, 36(4):943–955, 2024.
- Xin, L., Song, W., Cao, Z., and Zhang, J. Multi-Decoder Attention Model with Embedding Glimpse for Solving Vehicle Routing Problems. *AAAI*, 2021.
- Xin, L., Song, W., Cao, Z., and Zhang, J. NeuroLKH: Combining Deep Learning Model with Lin-Kernighan-Helsgaun Heuristic for Solving the Traveling Salesman Problem. *NeurIPS*, 2021.
- Xu, K., Li, J., Zhang, M., Du, S. S., Kawarabayashi, K., and Jegelka, S. What Can Neural Networks Reason About? *ICLR*, 2020.
- Zhou, J., Wu, Y., Song, W., Cao, Z., and Zhang, J. Towards Omni-generalizable Neural Methods for Vehicle Routing Problems. *ICML*, 2023.
- Zhou, J., Wu, Y., Cao, Z., Song, W., Zhang, J., and Shen, Z. Collaboration! Towards Robust Neural Methods for Routing Problems. *NeurIPS*, 2024.
- Zhou, J., Cao, Z., Wu, Y., Song, W., Ma, Y., Zhang, J., and Chi, X. MVMoE: Multi-Task Vehicle Routing Solver with Mixture-of-Experts. *ICML*, 2024.

A Formal View of the Local Consequence Comparator

This appendix formalizes the local consequence comparator. The results are intentionally local: they apply to the single-step candidate-comparison subproblem, not to the entire constructive MDP. The permutation-equivariant statements apply to the exchangeable customer rows in F ; the depot, when available, is a distinguished outside option rather than a customer row.

A.1 Common-mode decomposition. Fix a constructive step with $m = |F| > 0$ feasible customers. Let $X \in \mathbb{R}^{m \times p}$ collect their relative local-consequence features, with row x_j^\top for candidate j . Define $\mu(X) = \frac{1}{m} \sum_{j=1}^m x_j$ and $C(X) = X - \mathbf{1}\mu(X)^\top$. The centering map C is the canonical representative of the common-translation quotient: $C(X + \mathbf{1}\delta^\top) = C(X)$, and $C(X) = C(Y)$ iff $Y = X + \mathbf{1}\delta^\top$ for some $\delta \in \mathbb{R}^p$. It is also permutation equivariant: $C(PX) = PC(X)$. For any fixed candidate-shared weight w , logits $d_j = w^\top C(X)_j$ satisfy $d_j - d_k = w^\top (x_j - x_k)$, which is unchanged under $X \mapsto X + \mathbf{1}\delta^\top$; since softmax is invariant to candidate-independent shifts, the policy is unchanged. \square

A.2 Canonical equivariant linear local scorer. The following observation justifies the centered shared-linear form within the class of linear permutation-equivariant local scorers. Nonlinear candidate-wise alternatives are evaluated empirically in Section 4.4.

Fix $m = |F| > 1$ (for $m = 1$ the zero-mean gauge forces $\ell(X) = 0$ trivially). Consider a linear scorer $\ell : \mathbb{R}^{m \times p} \rightarrow \mathbb{R}^m$ on the relative consequence table X . Require that ℓ is (i) linear in X , (ii) permutation equivariant over candidates, and (iii) represented in the zero-mean softmax gauge, i.e. $\mathbf{1}^\top \ell(X) = 0$. Then there exists $w \in \mathbb{R}^p$ such that

$$\ell_j(X) = w^\top (x_j - \mu), \quad \mu = \frac{1}{m} \sum_{i=1}^m x_i. \quad (11)$$

Proof. Since ℓ is linear, each output logit can be written as $\ell_j(X) = \sum_{u=1}^m A_{j,u} x_u$ for row-to-logit linear functionals $A_{j,u} \in (\mathbb{R}^p)^*$. Permutation equivariance forces all diagonal blocks $A_{j,j}$ to equal a shared functional a^\top , and all off-diagonal blocks $A_{j,u}$ ($u \neq j$) to equal a shared functional b^\top . Hence $\ell_j(X) = a^\top x_j + b^\top \sum_{u \neq j} x_u$. The zero-mean gauge requires $\sum_j \ell_j(X) = 0$ for all X , giving $(a + (m-1)b)^\top \sum_j x_j = 0$, so $b = -\frac{a}{m-1}$. Substituting back and regrouping yields $\ell_j(X) = \frac{m}{m-1} a^\top (x_j - \mu)$. Setting $w = \frac{m}{m-1} a$ completes the proof. \square

This property justifies the LINC local branch as the canonical linear, permutation-equivariant, gauge-fixed scorer for relative deterministic consequences. The step-summary path handles the complementary candidate-common regime information. The degradation of centered MLP scoring in Table 5 is

consistent with this view: the MLP retains the centered coordinate but abandons the shared linear comparison geometry.

MDP interpretation: centering as a local advantage map. Suppose the contribution of the relative local consequences to the one-step logit is affine at a fixed state,

$$q_{\text{rel}}(s, j) = b(s) + w(s)^\top x_{\text{rel}}(s, j), \quad (12)$$

where $w(s)$ is shared across candidates at that step. The feasible-set average is

$$\bar{q}_{\text{rel}}(s) = b(s) + w(s)^\top \mu(s). \quad (13)$$

Thus

$$q_{\text{rel}}(s, j) - \bar{q}_{\text{rel}}(s) = w(s)^\top (x_{\text{rel}}(s, j) - \mu(s)). \quad (14)$$

Mean-centering therefore represents the local relative-feature contribution as an action advantage with a uniform-over-feasible-actions baseline. This is natural in a constructive MDP: it removes a component common to all candidate actions at the current state and keeps the feature deviations that affect the action ranking.

Scope. The result is weaker than full MDP bisimulation: single-step comparison optimality does not imply global multi-step optimality. In vehicle routing, a candidate that looks best locally can lead the vehicle into a dead-end region. LINC addresses this through its two-path design: the centered relative features $C_t(X_t)$ provide a provably invariant coordinate for candidate-specific local comparison, while the summary $r_t = [\rho_t, \text{mean}(\cdot), \min(\text{slack}/\text{load})]$ captures the global urgency of the current state. Through $\gamma_t, \beta_t, \alpha_t$, this summary modulates the decoder context, ensuring that the model does not greedily optimize local scores while ignoring whether the feasible set is shrinking, candidates are drifting far away, or time-window slack is running out. In short, the quotient map handles “which candidate is relatively better,” while the summary branch handles “how urgently should we respond to the current state.”

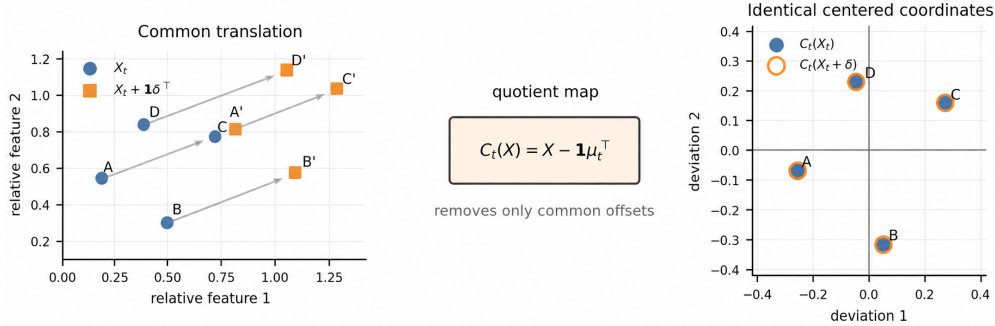


Figure 3: Set-relative centering as a quotient map. Although it may seem like common sense that subtracting the mean removes a shared offset, a learned model has no built-in notion of this structural invariance unless it is explicitly encoded. Two feature tables differing only by a common translation collapse to the same centered coordinates, while candidate-specific deviations are preserved.

B Solomon and TSPLIB Supplementary Results

This section provides per-instance breakdowns on external benchmarks. Solomon numerical tables use LINC SGBS results after distance matrix recovery, with protocol beam width 4, expansion size 4, 128 latent rollouts, and 8-fold augmentation; TSPLIB tables use 29 EUC_2D instances with integer-distance objectives.

Table 6: Per-instance Solomon56 results. HGS is the community best-known reference; other columns are evaluated in this repository. Values are route distances.

Instance	HGS	POMO-g	POMO-s	PolyNet	LINC	POMO-SGBS	PolyNet-SGBS	LINC-SGBS
C101	827.3	934.4	947.0	843.1	828.9	914.1	828.9	828.9
C102	827.3	1063.4	1073.9	953.7	831.5	1043.4	942.5	831.5
C103	826.3	1139.1	1141.4	1036.3	848.1	1125.8	939.7	838.7
C104	822.9	1156.3	1130.0	957.1	861.0	1075.3	910.7	860.2
C105	827.3	908.0	908.0	843.1	828.9	908.0	828.9	833.2
C106	827.3	1082.1	969.0	846.5	829.7	897.6	834.8	828.9
C107	827.3	1004.3	907.7	881.2	832.4	908.5	828.9	828.9
C108	827.3	1082.6	1059.9	843.7	835.4	968.1	834.8	828.9
C109	827.3	1034.7	1033.9	864.3	878.1	966.1	875.9	850.9
C201	589.1	861.6	823.5	766.5	646.7	815.2	657.9	614.9
C202	589.1	771.7	771.7	715.1	672.1	723.5	696.1	591.6
C203	588.7	916.8	865.6	761.5	645.5	842.9	703.2	593.9
C204	588.1	895.9	870.0	759.1	637.3	829.9	748.8	654.3
C205	586.4	837.9	809.2	689.2	590.5	790.3	610.3	588.9
C206	586.0	906.9	882.2	664.7	589.9	870.0	633.3	588.5
C207	585.8	771.1	760.1	658.2	604.3	718.5	636.3	589.3
C208	585.8	861.0	840.5	669.9	592.6	788.9	603.6	591.2
R101	1637.7	1885.7	1813.6	1794.0	1768.5	1770.0	1734.2	1714.7
R102	1466.6	1677.4	1652.4	1612.1	1564.4	1622.4	1573.9	1539.4
R103	1208.7	1456.2	1417.1	1390.1	1363.0	1422.7	1351.8	1314.8
R104	971.5	1198.2	1176.5	1110.0	1060.2	1120.7	1098.4	1040.8
R105	1355.3	1640.4	1643.0	1493.6	1486.7	1561.3	1455.7	1427.3
R106	1234.6	1554.5	1444.8	1363.0	1334.7	1418.5	1341.1	1325.8
R107	1064.6	1320.6	1263.2	1192.7	1178.6	1248.6	1170.5	1154.7
R108	932.1	1160.7	1127.2	1065.8	1001.5	1106.4	1035.0	999.6
R109	1146.9	1523.4	1420.8	1302.4	1262.4	1376.9	1265.0	1226.4
R110	1068.0	1308.2	1273.3	1187.3	1173.1	1278.1	1153.3	1144.7
R111	1048.7	1340.2	1250.4	1200.0	1143.0	1244.5	1187.7	1136.6
R112	948.6	1151.5	1113.8	1074.8	1025.3	1107.7	1041.7	1016.5
R201	1143.2	1343.9	1354.5	1275.9	1237.5	1292.3	1247.0	1212.9
R202	1029.6	1195.9	1208.1	1170.7	1104.6	1197.5	1124.0	1091.5
R203	870.8	1104.5	1072.6	987.4	937.9	1056.1	955.5	925.1
R204	731.3	883.1	865.3	803.8	767.3	877.1	794.4	763.0
R205	949.8	1188.9	1153.0	1077.3	1006.9	1158.9	1028.4	1005.0
R206	875.9	1069.3	1038.6	997.2	933.3	1045.2	957.1	923.8
R207	794.0	1004.7	966.3	918.6	857.5	966.5	866.7	845.3
R208	701.0	798.1	798.1	767.4	732.2	794.8	752.5	729.0
R209	854.8	1076.1	1017.6	957.2	901.3	1008.0	933.1	904.6
R210	900.5	1144.5	1048.0	1021.9	964.0	1055.2	992.1	935.1
R211	746.7	915.1	908.4	820.5	803.2	895.0	806.1	807.4
RC101	1619.8	2050.6	2044.3	1858.8	1794.3	1988.6	1732.2	1716.4
RC102	1457.4	1891.3	1846.6	1691.7	1574.6	1716.4	1580.9	1538.2
RC103	1258.0	1724.5	1611.3	1495.3	1401.5	1572.9	1405.1	1369.7
RC104	1132.0	1409.5	1384.5	1363.6	1248.7	1425.0	1288.2	1236.8
RC105	1513.7	1947.4	1934.4	1772.3	1695.8	1908.4	1666.1	1610.3
RC106	1372.7	1758.2	1706.1	1594.3	1494.2	1679.4	1482.1	1415.5
RC107	1207.8	1661.6	1591.1	1420.7	1360.1	1535.4	1390.0	1294.5
RC108	1114.2	1444.5	1409.5	1351.4	1267.6	1390.7	1292.9	1246.3
RC201	1261.8	1506.7	1527.2	1409.8	1329.5	1471.0	1354.3	1310.0
RC202	1092.3	1382.3	1303.8	1245.5	1142.6	1298.4	1179.3	1131.6
RC203	923.7	1164.8	1145.7	1085.1	986.2	1144.5	997.3	974.3
RC204	783.5	989.9	981.8	918.2	826.2	941.7	882.5	826.1
RC205	1154.0	1363.9	1392.6	1287.9	1227.4	1356.6	1265.9	1203.4
RC206	1051.1	1322.2	1214.4	1186.4	1120.4	1225.9	1159.2	1103.8
RC207	962.9	1350.2	1150.8	1111.3	1016.8	1162.3	1071.9	1014.7
RC208	776.1	1037.2	1012.6	909.6	825.9	968.6	857.7	816.0
Mean	973.2	1235.3	1197.8	1107.8	1044.1	1171.4	1064.0	1023.8

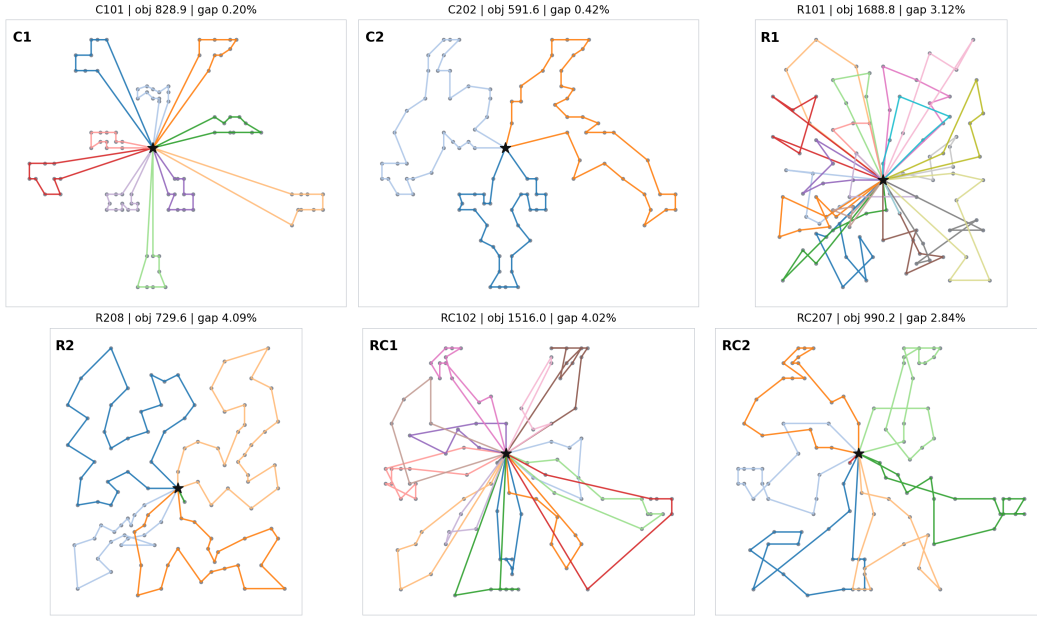


Figure 4: Representative LINC SGBS routes for the six Solomon instance classes.

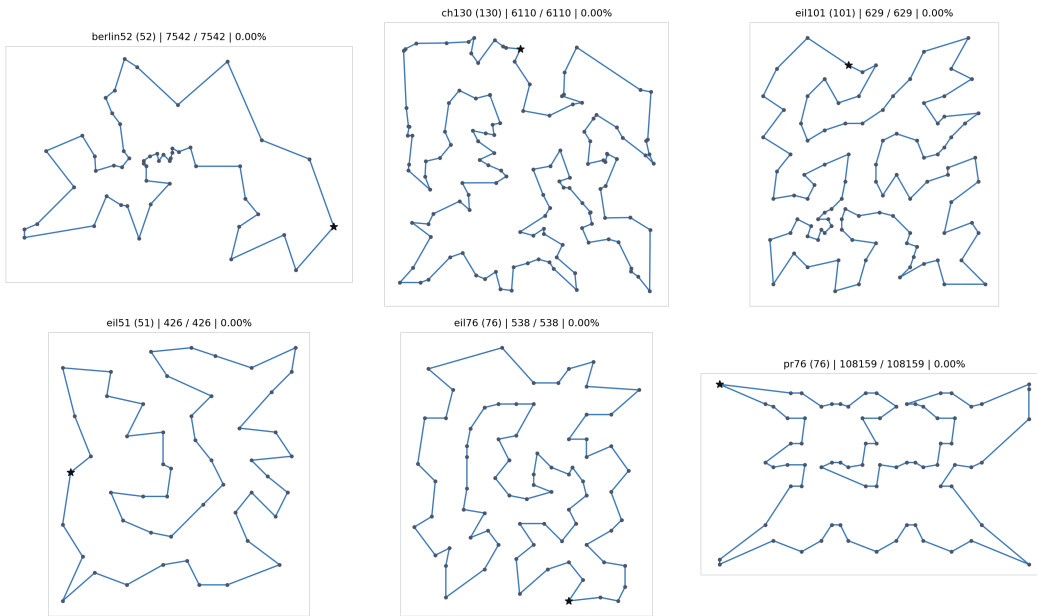


Figure 5: Six TSPLIB50–200 LINC SGBS tours with the lowest gap to the known optimum.

C Ablation Supplement: Full Table and Pairwise Comparisons

Table 8 reports the full ablation table including auxiliary encoder components. Figure 6 provides the pairwise training-score comparisons for all twelve ablation variants.

Table 7: Per-instance TSPLIB50–200 results. Values use EUC_2D integer distances.

Instance	n	Concorde	POMO-g	POMO-s	POMO-SGBS	PolyNet-SGBS	LINC-SGBS
berlin52	52	7542	7543	7543	7542	7542	7542
bier127	127	118282	136654	131273	122645	126686	120165
ch130	130	6110	6136	6119	6110	6110	6110
ch150	150	6528	6565	6557	6554	6528	6540
d198	198	15780	20016	18536	17543	18035	17427
eil101	101	629	632	630	629	629	629
eil51	51	426	428	428	428	426	426
eil76	76	538	541	538	538	538	538
kroA100	100	21282	21466	21367	21282	21282	21282
kroA150	150	26524	27131	26707	26528	26528	26528
kroA200	200	29368	30275	29829	29494	29624	29537
kroB100	100	22141	22399	22216	22199	22141	22141
kroB150	150	26130	26460	26460	26224	26189	26132
kroB200	200	29437	30364	29893	29536	29582	29478
kroC100	100	20749	20987	20789	20749	20749	20749
kroD100	100	21294	21513	21472	21309	21294	21374
kroE100	100	22068	22381	22173	22120	22079	22068
lin105	105	14379	14782	14449	14379	14379	14379
pr107	107	44303	45927	44537	44351	44482	44891
pr124	124	59030	59827	59390	59076	59076	59030
pr136	136	96772	98180	97792	97420	96781	97105
pr144	144	58537	59574	58766	58588	59348	58537
pr152	152	73682	74455	74167	73690	73922	73848
pr76	76	108159	108308	108159	108159	108159	108159
rat195	195	2323	2675	2524	2407	2391	2358
rat99	99	1211	1266	1232	1215	1213	1212
rd100	100	7910	7919	7910	7910	7910	7910
st70	70	675	675	675	676	675	676
u159	159	42080	42773	42512	42411	42080	42291
Mean	–	30478.9	31650.1	31194.6	30748.7	30909.6	30657.3

Table 8: Full ablation including auxiliary encoder components. Rel. gap is measured relative to Full LINC within the same simplified CVRPTW ablation setting.

Variant	Local cons.	GateAttn	Depth Mixer	Credit	Obj.	Rel. gap
Baseline	N	N	N	original	631.65	6.66%
Full LINC	Y	Y	Y	soft top-1	592.21	0.00%
w/o local cons. interface	N	Y	Y	soft top-1	605.60	2.26%
Naive MLP injection	MLP only	Y	Y	soft top-1	605.89	2.31%
w/o GateAttn	Y	N	Y	soft top-1	592.06	−0.03%
w/o Depth Mixer	Y	Y	N	soft top-1	600.73	1.44%
w/o soft top-1	Y	Y	Y	hard top-1	595.59	0.57%
group_mean	Y	Y	Y	group_mean	626.37	5.77%
Centered MLP scoring	centered MLP	Y	Y	soft top-1	608.98	2.83%
Raw linear scoring	raw linear	Y	Y	soft top-1	593.66	0.25%
w/o step summary	Y	Y	Y	soft top-1	610.85	3.15%
Full mean summary	Y	Y	Y	soft top-1	594.91	0.46%

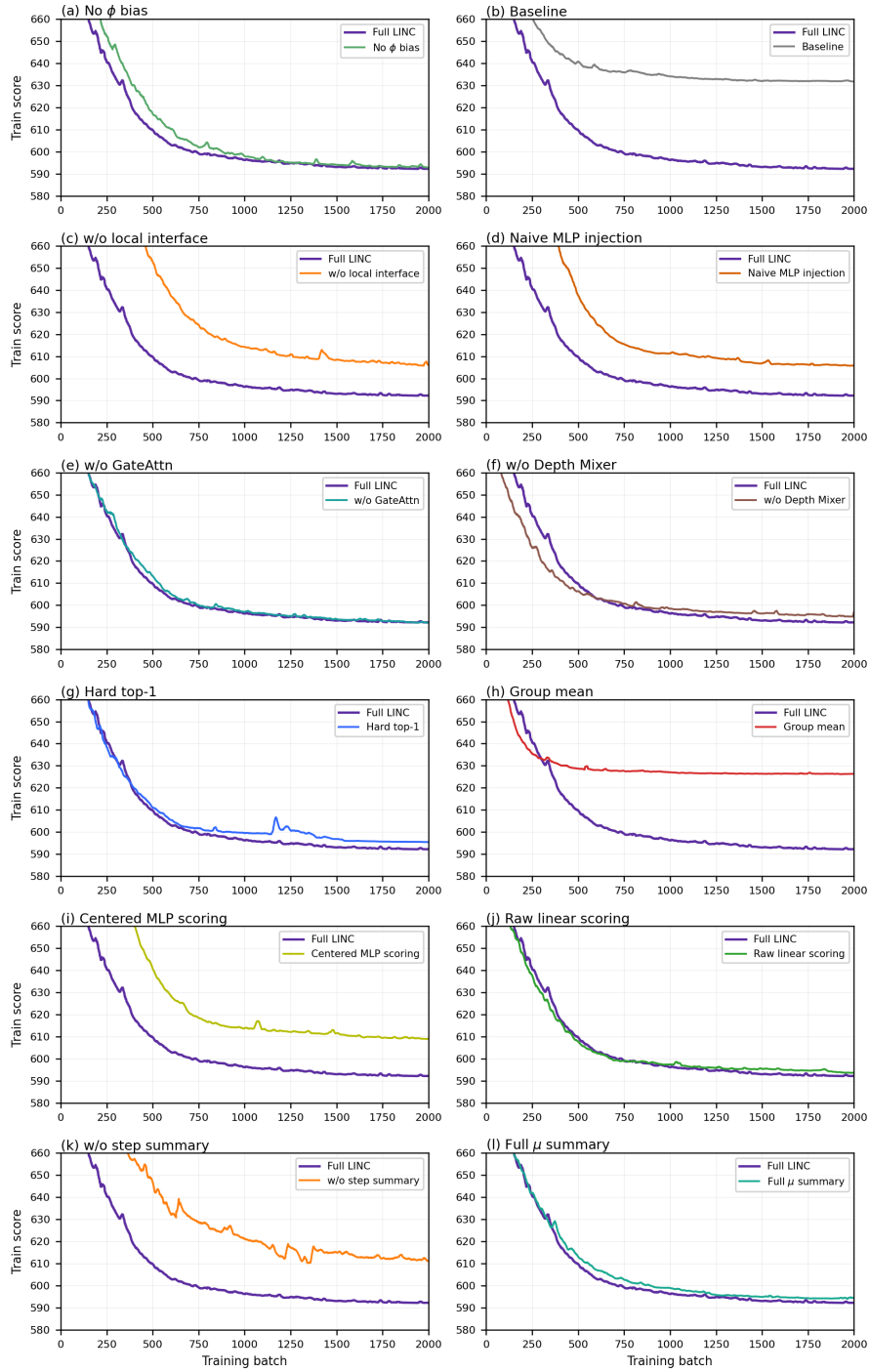


Figure 6: Pairwise training-score comparisons for all ablation variants on the simplified dataset. The full LINC reference curve is shown against each variant over the full training budget.

D Budget Sensitivity and Statistical Checks

Reduced-budget decoding ($z=400$). Table 9 evaluates LINC with the latent/sample budget reduced from the main setting $z = 800$ to $z = 400$ while increasing batch size where memory permits. The first five rows are random or in-distribution checks; the remaining rows are external benchmarks. The table reports PolyNet $z = 800$, LINC $z = 400$, and LINC $z = 800$ side by side so that both quality and wall-clock time can be compared directly. The purpose is not to claim wall-clock dominance on every saturated benchmark, but to check whether the observed improvements require simply decoding more trajectories. The reduced-budget setting remains close to the main results and retains the external/CVRPTW advantage in the settings where the paper’s main claim is strongest.

Table 9: Reduced-budget check for LINC. All metrics are objective values (lower is better). PolyNet and LINC main ($z = 800$) values are from the main result tables; wall-clock times are listed next to each objective for direct comparison.

Role	Dataset	PolyNet $z = 800$		LINC $z = 400$		LINC $z = 800$	
		Obj.	Time	Obj.	Time	Obj.	Time
Random / in-dist.	TSP100	7.765	4m	7.765	4m	7.765	8m
	TSP150	9.352	1m	9.353	1m	9.352	2m
	CVRP100	15.640	5m	15.646	5m	15.638	9m
	CVRP150	19.507	2m	19.483	1m	19.468	3m
	CVRPTW synthetic100	2016.5	6m	1924.6	6m	1920.4	12m
External	CVRPXML100	17632.2	7m	17551.4	8m	17518.8	14m
	Solomon56	1107.8	3s	1049.0	3s	1043.9	6s
	Homburger200	3712.8	8s	3103.5	8s	3083.0	15s
	TSPLIB50–200	31474.2	17s	31253.4	12s	31096.3	17s

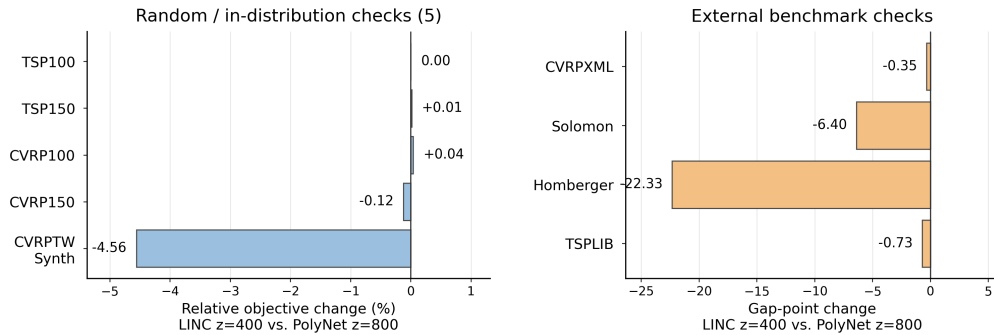


Figure 7: Reduced-rollout sensitivity for LINC $z = 400$ relative to PolyNet $z = 800$. The left panel contains the five random/in-distribution checks, while the right panel contains external benchmarks with TSPLIB placed on the right-side external group. Negative values favor LINC; TSP150 and CVRP100 are the only reduced-budget checks where LINC is slightly worse.

Paired bootstrap on small-margin random benchmarks. For the saturated TSP/CVRP random benchmarks, the absolute margins over PolyNet are small by construction. We therefore report paired bootstrap intervals over test instances with three pre-specified evaluation seeds (1234, 42, 2026) under fixed checkpoints. These intervals capture instance-level variability of the LINC–PolyNet difference and confirm that the improvement is consistent across seeds. All intervals are negative (LINC lower cost), and none cross zero.

Table 10: Paired bootstrap checks for small residual-gap comparisons. The reported difference is LINC minus PolyNet; lower is better, so a negative interval favors LINC.

Benchmark	Seed	LINC	PolyNet	Diff.	95% CI
TSP random150	1234	9.3518	9.3528	−0.00104	[−0.00139, −0.00070]
TSP random150	42	9.3516	9.3527	−0.00105	[−0.00142, −0.00068]
TSP random150	2026	9.3519	9.3527	−0.00082	[−0.00118, −0.00047]
CVRP random100	1234	15.6380	15.6402	−0.00221	[−0.00286, −0.00154]
CVRP random100	42	15.6379	15.6401	−0.00219	[−0.00284, −0.00156]
CVRP random100	2026	15.6380	15.6400	−0.00193	[−0.00257, −0.00130]

E Training Hyperparameters

All tasks use Adam optimizer ($\beta_1 = 0.9$, $\beta_2 = 0.999$, weight decay 10^{-6}) with amp mixed precision, learning rate 10^{-4} , batch size 128, and rollout width $K = 128$. Each epoch contains 6400 training instances. For CVRPTW’s matched soft top-1, τ decays exponentially from 4.0 to 0.25 (decay ratio 1/16, completed within $\approx 1/300$ epochs), with cost scale factor s set to the batch median. TSP and CVRP anneal λ_{morph} from 0 to 1 over the first 100 epochs. Models are trained for approximately 300 (TSP), 1400 (CVRP), and 12000 (CVRPTW) epochs respectively. Training uses a single NVIDIA RTX 5090 32GB GPU; evaluation uses a single A100 40GB GPU.

F Data Generation Details

Existing NCO training distributions for CVRPTW can be narrow—restricted to limited spatial layouts, loose time windows, or nearly uniform constraint densities—which makes external benchmark transfer difficult. We therefore design a procedural generator that covers a broader instance envelope through explicit rule-based sampling over spatial morphology, temporal coupling, and constraint intensity. The distribution spans loosely constrained to tightly coupled instances and is not explicitly fitted to Solomon or Homberger statistics. For each instance, we first sample latent variables

$$z = \{S, H, \nu, \alpha, K, \pi^{\text{space}}, \pi^{\text{width}}, \pi^{\text{phase}}, r_{\text{con}}\}, \quad (15)$$

where S is the spatial scale, H the time horizon ratio, ν the service time ratio, α the distance-to-time scaling coefficient, K the number of clusters, π^{space} , π^{width} , and π^{phase} are mixture weights for spatial, time-window width, and phase components, respectively, and r_{con} is the proportion of constrained nodes. The time horizon endpoint and service time are defined as

$$T_{\text{max}} = HS, \quad s = \nu S. \quad (16)$$

On the normalized plane $[0, 1]^2$, customer locations are generated by mixing four spatial component types: clustered Gaussian components, uniform components, banded corridor components, and outlier components. Let \tilde{x}_j be the normalized position; the absolute coordinate is

$$x_j = S\tilde{x}_j. \quad (17)$$

Outlier components are explicitly constrained to be far from the depot and main cluster centers, ensuring that the training envelope includes long-distance, low-density, and non-uniform structures.

For time-window generation, we first compute the feasible upper and lower bounds for each node based on travel time from the depot. Let the depot coordinate be x_0 ; then

$$\Delta_j = \alpha \|x_j - x_0\|_2, \quad (18)$$

$$L_j = \Delta_j, \quad U_j = T_{\text{max}} - \Delta_j - s. \quad (19)$$

Here L_j ensures the vehicle can reach the customer from the depot; U_j ensures sufficient time remains to return to the depot after service.

We then construct normalized phase variables for each node. Let ψ_j^{cluster} , ψ_j^{radial} , ψ_j^{angular} , ψ_j^{rand} denote cluster, radial, angular, and random phases, and π^{phase} be the 4-dimensional weight vector:

$$p_j = \text{clip} \left(\sum_{q \in \{\text{cluster}, \text{radial}, \text{angular}, \text{rand}\}} \pi_q^{\text{phase}} \psi_j^q + \epsilon_j, 0, 1 \right), \quad (20)$$

with $\epsilon_j \sim \mathcal{N}(0, \sigma_p^2)$. Each node is marked as constrained with probability r_{con} , otherwise unconstrained.

For unconstrained nodes, the time window is set to a global wide window or approximately global wide window. For constrained nodes, we use the phase variable to determine the window center:

$$m_j = L_j + p_j(U_j - L_j), \quad (21)$$

then sample from narrow, medium, and loose Beta width distributions:

$$\omega_j \sim \sum_{r \in \{\text{narrow}, \text{medium}, \text{loose}\}} \pi_r^{\text{width}} \text{Beta}(a_r, b_r), \quad (22)$$

with window width

$$W_j = \max\{w_{\min}, \omega_j(U_j - L_j)\}. \quad (23)$$

The final time window is

$$e_j = \max\{L_j, m_j - \frac{1}{2}W_j\}, \quad l_j = \min\{U_j, m_j + \frac{1}{2}W_j\}. \quad (24)$$

This generator thus creates a continuously controllable instance envelope across three dimensions—spatial morphology, temporal coupling structure, and constraint intensity—to improve coverage of heterogeneous CVRPTW characteristics without explicitly fitting a specific benchmark’s statistics.

G Encoder Auxiliary Refinements

The encoder uses two lightweight auxiliary components inherited from the base architecture:

GateAttn. Multi-head attention outputs are modulated by head-level gates $g_{v,h}^{(\ell)} = 2\sigma(W_g z_v^{(\ell-1)} + b_g)_h$, producing gated outputs $\hat{o}_{v,h}^{(\ell)} = (1 - \lambda_{\text{gate}})o_{v,h}^{(\ell)} + \lambda_{\text{gate}}g_{v,h}^{(\ell)}o_{v,h}^{(\ell)}$. Gates centered at 1 allow both suppression and enhancement.

Depth Mixer. Representation history across encoder layers is aggregated via learned depth queries $q^{(\ell)}$, computing attention weights $\omega_{n,m}^{(\ell)} \propto \exp(\text{Norm}(v_n^{(m)}), q^{(\ell)})$ over past layer outputs, with aggregated input $\hat{h}_n^{(\ell)} = \sum_{m < \ell} \omega_{n,m}^{(\ell)} \text{Norm}(v_n^{(m)})$.

Main-text Table 5 focuses on decoder-side LINC ablations; the full table below additionally reports auxiliary encoder ablations. Removing GateAttn is neutral (−0.03%) and removing Depth Mixer costs 1.44%, which is smaller than removing the local-consequence interface (2.26%), the shared linear comparator structure (2.83%), or the step-level summary (3.15%). This supports their role as auxiliary implementation refinements rather than the source of LINC’s main gains.

H Matched Soft Top-1 Advantage Derivation

Let $\hat{c}_i = c_i/s$ be scaled costs, $s_i = -\hat{c}_i/\tau$ be scaled logits, $m_{\text{all}} = -\tau \log(\frac{1}{K} \sum_j e^{s_j})$, $m_{\text{loo}}(i) = -\tau \log(\frac{1}{K-1} \sum_{j \neq i} e^{s_j})$. As $\tau \rightarrow \infty$, $s_j \rightarrow 0$, and a Taylor expansion $e^{s_j} \approx 1 + s_j$ gives:

$$m_{\text{all}} \approx -\tau \cdot \frac{1}{K} \sum_j s_j = \frac{1}{K} \sum_j \hat{c}_j, \quad (25)$$

$$m_{\text{loo}}(i) \approx -\tau \cdot \frac{1}{K-1} \sum_{j \neq i} s_j = \frac{1}{K-1} \sum_{j \neq i} \hat{c}_j. \quad (26)$$

Therefore

$$A_i = (K-1)(m_{\text{loo}}(i) - m_{\text{all}}) \approx (K-1) \left(\frac{1}{K-1} \sum_{j \neq i} \hat{c}_j - \frac{1}{K} \sum_j \hat{c}_j \right) = \frac{1}{K} \sum_j \hat{c}_j - \hat{c}_i, \quad (27)$$

which recovers the POMO-style advantage with a group-mean baseline (up to a constant factor s^{-1}). The $(K-1)$ factor ensures that the advantage maintains the correct scale at finite τ : without it, the softened advantage magnitude decays as K grows, compressing early training signals.

I Mechanism Diagnostics

We include lightweight diagnostics on the trained CVRPTW checkpoint under the Solomon56 evaluation protocol, inspecting whether the implemented candidate scorer behaves according to the mechanism assumed in the main text.

Common-translation probe. For each feasible set, we fix the decoder state and mask and add a shared offset to all local relative features. Figure 8 compares the centered comparator with the same affine comparator without centering under the clipped-softmax decoder. The centered scorer stays invariant up to numerical precision, while the uncentered scorer produces visible probability drift and top-1 flips as the shared offset grows.

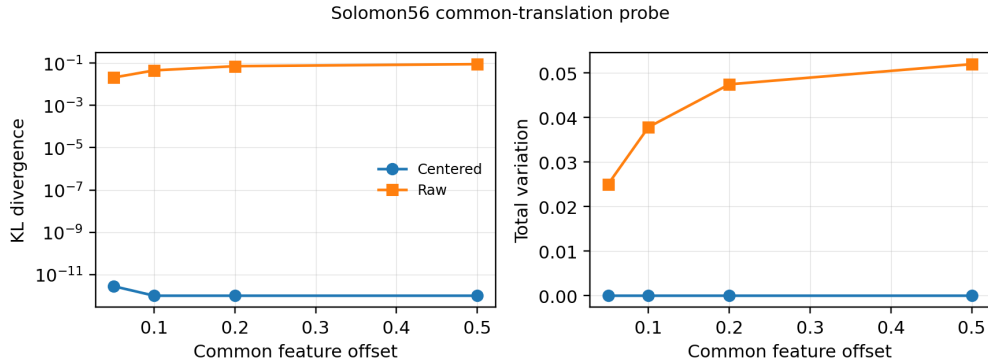


Figure 8: Common-translation probe on Solomon56. Centered local comparison is effectively invariant to shared feature offsets, whereas the uncentered affine comparator changes after logit clipping.

Adaptive modulation. Figure 9 shows that the learned summary gate α_t remains active through early and middle decoding, while the local-score share decreases near the end of the route when fewer feasible choices remain. This is consistent with the intended separation: the centered local comparator ranks candidate-specific consequences, and the summary branch calibrates how strongly those consequences influence the current step.

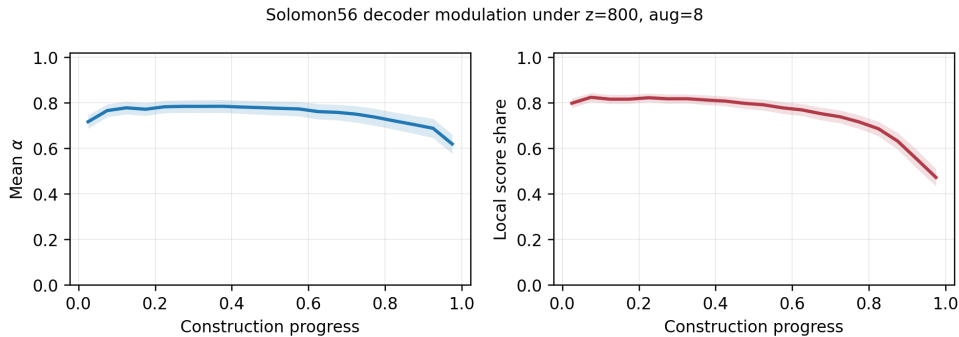


Figure 9: Summary modulation diagnostics on Solomon56. The learned gate and local-score share vary with construction progress rather than acting as a fixed feature-injection layer.

Feature roles. Figure 10 groups local-comparator weights by feasible-set size. Travel remains the dominant local consequence, while wait, arrival, departure, and angular terms become stronger when the feasible set is small. This matches the CVRPTW intuition that the model first avoids unnecessary travel, then increasingly values temporal urgency as feasible options disappear.

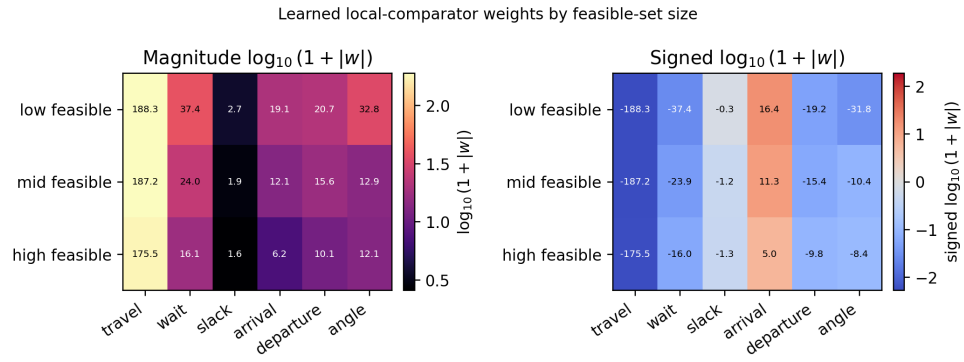


Figure 10: Local-comparator feature weights grouped by feasible-set size. Temporal features gain relative importance when fewer customers remain feasible.